

Adsorption of tris(8-hydroxyquinoline)aluminum molecules on cobalt surfaces

Yun-Peng Wang and Xiu-Feng Han

Beijing National Laboratory of Condensed Matter Physics, Institute of Physics, Chinese Academy of Sciences, Beijing 100190, China

Yu-Ning Wu and Hai-Ping Cheng

Department of Physics and Quantum Theory Project, University of Florida, Gainesville, Florida 32611, USA

(Received 7 August 2011; revised manuscript received 7 April 2012; published 27 April 2012)

We studied the adsorption of tris(8-hydroxyquinoline)aluminum (Alq_3) molecules on cobalt surfaces using density functional theory with the generalized gradient approximation. The van der Waals interaction between Alq_3 molecules and cobalt surfaces was included by the dispersion correction. Magnetization of Alq_3 molecules, adsorption energies, and bonding energies were obtained for smooth and defective surfaces and for various molecule-surface configurations. Electronic structures were analyzed for states that are relatively stable. We found that both the permanent electric dipole of Alq_3 molecules and the charge redistribution near the interface contribute to the interface dipole, and the interface dipole due to charge redistribution is important to determine the work function of a Co/ Alq_3 surface. Our calculated energy-level alignment at interfaces is consistent with experimental observations.

DOI: 10.1103/PhysRevB.85.144430

PACS number(s): 68.43.Bc

I. INTRODUCTION

Since the discovery and revolutionary applications of giant magnetoresistance¹ and tunnel magnetoresistance² in information technology, scientists and engineers have been interested in spin-dependent transport properties of organic semiconductors. The weak spin-orbit interactions in π -conjugated organic molecules compared to inorganic semiconductors make these molecules promising candidates for future spintronics.^{3,4}

At low temperatures, relatively large magnetoresistance was observed in typical organic magnetic junctions where Alq_3 molecules were used as nonmagnetic spacer layers.^{4–7} Magnetoresistance has also been observed at room temperature,^{8–10} but it decreases sharply as the temperature increases. The reported performance of magnetic junctions with Alq_3 molecules as spacer is widely variable, and both positive⁵ and negative¹⁰ magnetoresistances were observed. This uncertainty reflects difficulties in making organic magnetic junctions. Compared to inorganic spacer layers (for instance, AlO_x and MgO) for which the interfaces between magnetic electrodes and spacer layers can be efficiently improved by high-temperature annealing, organic molecules interact via weak van der Waals interactions, such that there is no ideal approach to improve and optimize either the texture of molecule layers or the interfaces between the molecule spacer and the two electrodes. Especially when depositing metal atoms on organic layers to grow an electrode, the quality of the interface is largely affected by strong atom-molecule interactions, atomic interfacial diffusion, and even pinholes,¹¹ although some techniques have been employed to prevent the diffusion of metal atoms into organic layers.^{12,13} Chemical interactions between Alq_3 molecules and transition-metal surfaces have been probed by spectroscopy methods.^{14–16}

The electronic structure at interfaces between organic molecules and metallic electrodes, especially the alignment of energy levels of molecules and the Fermi level of metal electrodes, is critical for charge and spin injection.¹⁷ Metals with low work functions have been widely used as negative

electrodes in electroluminescence devices¹⁸ to decrease the hole-injection energy barrier. For these reasons, the adsorption geometries, interface dipoles, and energy-level alignments at interfaces between Alq_3 molecules and low-work-function metals such as aluminum, calcium, and magnesium were studied extensively.^{19–25} In organic spin valves, the interfacial orbital hybridizations between the first layer of organic molecules and magnetic electrodes plays a key role in spin injection.⁵ Strong hybridization may change the sign of the spin polarization of magnetic surfaces.¹⁷ Barraud *et al.*⁵ argued that the Alq_3/Co interface is in the weak-coupling regime and positive spin polarization of the cobalt surface is not reversed by Alq_3 molecule adsorption. The energy barrier of hole (electron) injection is the energy difference between the highest occupied molecular orbital (HOMO) [lowest unoccupied molecular orbital (LUMO)] level and the Fermi level of the electrodes. If there is no interface dipole, the energy-level alignment is determined by the vacuum energy-level alignment rule. Otherwise, energy levels of molecule orbitals shift in the presence of an interface dipole and energy-level alignment is determined by the interface dipole. There are several proposed mechanisms for the formation of the interface dipole.²⁶ The injection barriers of holes at interfaces between Alq_3 and cobalt¹⁵ or iron²⁷ were determined by photoelectron spectroscopy methods and the position of the LUMO energy level of the Alq_3 molecule was deduced from the HOMO-LUMO gap. Recently, both HOMO and LUMO energy levels at surfaces were directly determined by ballistic-electron-emission spectroscopy²⁸ and energy-level alignments at Alq_3/Fe and Alq_3/Al interfaces were measured. Spin polarization of molecule orbitals in Alq_3 adsorbed on cobalt and iron was studied by *ab initio* methods.²⁷ However, a systematic study of interface dipole and electronic structure at different $\text{Alq}_3/\text{transition-metal}$ interfaces is still lacking. In this work, we focused on interfaces between Alq_3 molecules and smooth cobalt surfaces as well as cobalt surfaces with simple defects. In experiments, cobalt was widely used as the magnetic electrodes in Alq_3 -molecule-based organic

spin valves.^{4,5,8,9,12,29} Organic spintronics devices using Alq₃ molecules as spacer and cobalt as magnetic electrode were successfully prepared^{4,5,8–10,12} and large magnetoresistances were observed across these metal-organic-metal junctions. In experiments, both hcp(0001) and fcc(111) surfaces of cobalt were observed in thin films deposited by the evaporation method.³⁰ In our calculations we studied adsorption of Alq₃ molecules on a cobalt hcp(0001) surface, but we expect that our results can also shed light on the fcc(111) surface due to the similarity between cobalt hcp(0001) and fcc(111) surfaces.

The aim of this work is to investigate the interface electronic structure and energy-level alignment of Alq₃ on smooth and defective cobalt surfaces. In Sec. II a brief introduction of the first-principles method used in this work is given. In Sec. III, we present our calculated results concerning adsorption geometries, energies, work functions, charge transfers, and magnetic properties of Alq₃ molecules on cobalt surfaces. In Sec. IV, a detailed analysis on interface dipoles and spin-polarized electronic structures is presented.

II. METHOD OF CALCULATION

In this work, first-principles calculations based on density functional theory in the plane-wave basis were carried out using the PWSCF program in the QUANTUM ESPRESSO package³¹ employing the generalized gradient approximation (GGA) for exchange-correlation potentials as parametrized by Perdew, Burke, and Ernzerhof.³² Interactions between valence electrons and ions were treated by ultrasoft GGA pseudopotentials³³ implemented in QUANTUM ESPRESSO.³⁴ To simulate isolated Alq₃ molecules, a 26.5 × 26.5 × 22.5 Å³ supercell was used so that interactions between neighboring molecules are negligible. To minimize surface-surface interactions, a slab with seven layers was used to simulate the surface of cobalt with 6 × 6 cobalt atoms in each layer. The positions of cobalt atoms in the bottom three layers were kept fixed at their locations in the bulk phase during geometry relaxation. We chose the direction perpendicular to the cobalt surface as the *z* axis. Lattice constants of hexagonal close-packed (hcp) cobalt were measured by the x-ray Bond method³⁵ to be *a* = 2.503 Å and *c/a* = 1.621 at low temperature. We obtained the same lattice constant with experimental results by GGA calculations. In the *z* direction a vacuum region of 1.2 nm was inserted to separate two adjacent slabs. Ground states and total energies of all systems were obtained after full geometry relaxation with forces on atoms smaller than 25 meV/Å and total energy within 15 meV per unit cell. Löwdin orthogonalization and population analysis^{36,37} were used to extract the magnetic moments of atoms and charge transfer between molecule and surface. Because the slab with molecules adsorbed on one surface is asymmetric, the dipole correction approach³⁸ was used.

For adsorption of molecules on metal surfaces, the inclusion of van der Waals interactions has been shown to be important to predict adsorption energies and geometries,^{39–43} especially for Alq₃ molecule adsorption on metals.^{23,25} A review of techniques for computing van der Waals interactions

in density functional theory (DFT) is given in Ref. 44. Dispersion-corrected DFT^{45–49} (DFT-D) was among the most popular schemes to incorporate the van der Waals interaction into density functional theory before the emergence of the parameter-free van der Waals density functional^{50–52} (vdW-DF) method, which accounts for van der Waals interactions using a correlation term that is a nonlocal functional of electron density. The vdW-DF method was used to calculate adsorption of Alq₃ molecules on nonmagnetic metal surfaces such as Al (Ref. 23) and Mg (Ref. 25). However, the extension of the vdW-DF method to spin-polarized problems is not completed yet, and there is no reliable vdW-DF method for studying adsorption of Alq₃ molecules on a spin-polarized cobalt surface. Therefore, we used the DFT-D scheme in this paper to include van der Waals interaction.

In the DFT-D method the total energy is

$$E_{\text{tot}} = E_{\text{DFT}} - s_6 \sum_{i=1}^N \sum_{j>i}^N f(S_R R_{ij}^0, R_{ij}) C_{ij} R_{ij}^{-6}, \quad (1)$$

where E_{DFT} is the uncorrected DFT total energy. The second term on the right-hand side is the dispersion correction to the total energy, where R_{ij} is the distance between atom *i* and atom *j*, s_6 and S_R are global parameters, and R_{ij}^0 and C_{ij} are parameters for an atom pair (*i*, *j*).

There are different schemes and implementations proposed for the DFT-D method, as reviewed in Refs. 43 and 53. Among them, the Grimme implementation⁴⁸ gave parameters for most elements in the periodic table, which we adopt in this paper. In the Grimme DFT-D scheme,⁴⁸ the damping function $f(r_0, r)$ in Eq. (1) takes the form

$$f(r_0, r) = \frac{1}{1 + e^{-d(r/r_0-1)}}, \quad (2)$$

with $d = 20$ in Eq. (2) and $S_R = 1$ in Eq. (1). The global scaling parameter s_6 depends on the exchange-correlation functional used and $s_6 = 0.75$ for Perdew-Burke-Ernzerhof (PBE) parametrization.³² Therefore, Eq. (1) becomes

$$E_{\text{tot}} = E_{\text{DFT}} - 0.75 \sum_{i=1}^N \sum_{j>i}^N \frac{C_{ij} R_{ij}^{-6}}{1 + e^{-20[R_{ij}/(R_i + R_j) - 1]}}, \quad (3)$$

where R_i and R_{ij} are van der Waals radii for atom *i* and distances between atoms *i* and *j*, respectively. The C_{ij} coefficients are given by the following combination rule:

$$C_{ij} = \sqrt{C_i C_j}. \quad (4)$$

The van der Waals radii R_i and coefficients C_i for elements in the periodic table up to xenon are given in Ref. 48.

III. RESULTS

There are two isomers of the Alq₃ molecule, facial and meridional (see Fig. 1).^{54,55} Geometries of both isomers in the

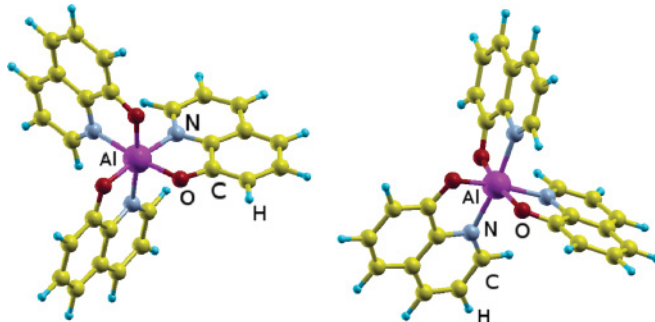


FIG. 1. (Color online) Structures of Alq_3 molecule isomers. Three oxygen atoms and three nitrogen atoms are at the vertices of an octahedron, and an aluminum atom sits at the center. In the facial Alq_3 isomer (left), the three oxygen atoms form a regular triangle. Two of the three oxygen atoms are located on opposite sites of the center aluminum atom in the meridional isomer (right).

isolated state were obtained after full structural relaxation. The calculated bond lengths between two atoms (as shown in Table I) in Alq_3 isomers agree well with experimental results^{55,56} and are consistent with previous calculation results.^{54,57,58} Both Alq_3 isomers are polar molecules, with intrinsic electric dipoles. The dipole moments of the facial and meridional isomers calculated by the GGA method are 7.2 and 4.0 D, respectively, which are close to previous calculations (6.9 D for facial and 3.9 D for meridional isomers, respectively);²² however, these numbers are slightly smaller than 7.9 D for the facial isomer and 5.3 D for the meridional isomer found by hybrid DFT Becke three-parameter Lee-Yang-Parr (B3LYP) methods.⁵⁹ A crystal phase of meridional Alq_3 can be obtained after thermal annealing of a facial isomer crystal,⁶⁰ which indicates that the meridional isomer is more thermally stable than the facial isomer.⁶¹ In this work, the total energy of the facial Alq_3 molecule was calculated to be 0.17 eV higher than that of the meridional isomer, which is similar to the previous GGA BLYP results,⁶² but smaller than hybrid DFT B3LYP results.^{59,63} The DFT-D results for

TABLE I. Lengths of N-Al and O-Al bonds in facial and meridional Alq_3 molecules relaxed by the GGA method (in angstroms). The experimental results are determined by x-ray diffraction methods.^{55,57} Bond lengths of the meridional isomer are taken from Ref. 57 and those of the facial isomer are taken from δ -phase crystal.⁵⁵ The GGA density functional calculation results are taken from Refs. 58 (meridional isomer) and 54 (facial isomer).

Bond length	GGA (this work)	GGA (other calculations)	Experimental results
Meridional			
Al-O1	1.89	1.89	1.86
Al-O2	1.89	1.89	1.86
Al-O3	1.86	1.87	1.85
Al-N1	2.12	2.10	2.09
Al-N2	2.08	2.06	2.05
Al-N3	2.06	2.05	2.02
Facial			
Al-O	1.86	1.85	1.88
Al-N	2.13	2.15	2.14

structures, electric dipoles, and total energy difference between facial and meridional Alq_3 isomers are identical to the GGA results.

In the fully relaxed cobalt slab, the distance between the top surface layer and the subsurface layer was calculated to be 0.06 Å shorter than in the bulk phase, while the second-layer spacing was 0.04 Å longer. Magnetic moments of cobalt atoms on the top surface were calculated to be $1.74\mu_B$, which is about $0.1\mu_B$ larger than that of cobalt atoms in the bulk phase. The enhancement of magnetization at the surface is consistent with the previous result.⁶⁴ The work function of the smooth cobalt surface as defined by the difference between the Fermi energy and the electrostatic potential (multiplied by the charge of an electron) far away from the surface was calculated to be 5.0 eV, which is in good agreement with experimental results.⁶⁵

It was observed from experiments¹⁴ that Alq_3 molecules tend to contact with cobalt surfaces via oxygen atoms. Electric dipoles of Alq_3 point from oxygen atoms to the aluminum atom. According to experimental observations,¹⁴ Alq_3 isomers take “up” configurations on cobalt surfaces, i.e., with their electric dipole pointing from the cobalt surface to vacuum. For completeness, we have considered both “up” and “down” configurations, where the electric dipoles of Alq_3 molecules point from vacuum to the cobalt surface. In the initial states before structure relaxation, facial or meridional Alq_3 molecules were placed on top of the cobalt surface with three or two oxygen atoms facing the surface in the “up” configuration (fac-up and meri-up) and three or two nitrogen atoms facing the cobalt surface in the “down” configuration (fac-down and meri-down). Surfaces of cobalt thin films, especially deposited on soft organic substrate, are not defect-free. In this study, the two most simple point defects, surfaces with a single adatom and with a single vacancy, were taken into account. Each adsorption configuration can be labeled by a three-word combination; e.g., “fac-up/adatom” stands for facial Alq_3 molecule in the up configuration on a cobalt surface with an adatom (see Fig. 2).

The most stable adsorption configurations were obtained by full geometry relaxation, and the adsorption energy is defined as

$$E_{\text{ad}} = E_{\text{mol}} + E_{\text{surf}} - E_{\text{mol+surf}}, \quad (5)$$

where E_{mol} , E_{surf} , and $E_{\text{mol+surf}}$ are the total energies of Alq_3 molecules in the gas phase, of a free cobalt surface, and of the most stable adsorption configuration, respectively.

The energy of chemical bonds formed between Alq_3 molecules and a cobalt surface is another quantity that is useful to analyze interactions. The definition of bonding energy E_b is similar to that of adsorption energy:

$$E_b = E'_{\text{mol}} + E'_{\text{surf}} - E_{\text{mol+surf}}, \quad (6)$$

where E'_{mol} and E'_{surf} are the total energies of the Alq_3 molecule and the cobalt surface. In calculating E'_{mol} and E'_{surf} , atomic positions were taken from the most stable adsorption configuration. Configurations of both the Alq_3 molecule and the cobalt surface distort after molecular adsorption on the surface. As a result, E'_{mol} or E'_{surf} is the sum of E_{mol} or E_{surf} and the corresponding distortion energy. Obviously, bonding energy is larger than adsorption energy. In addition,

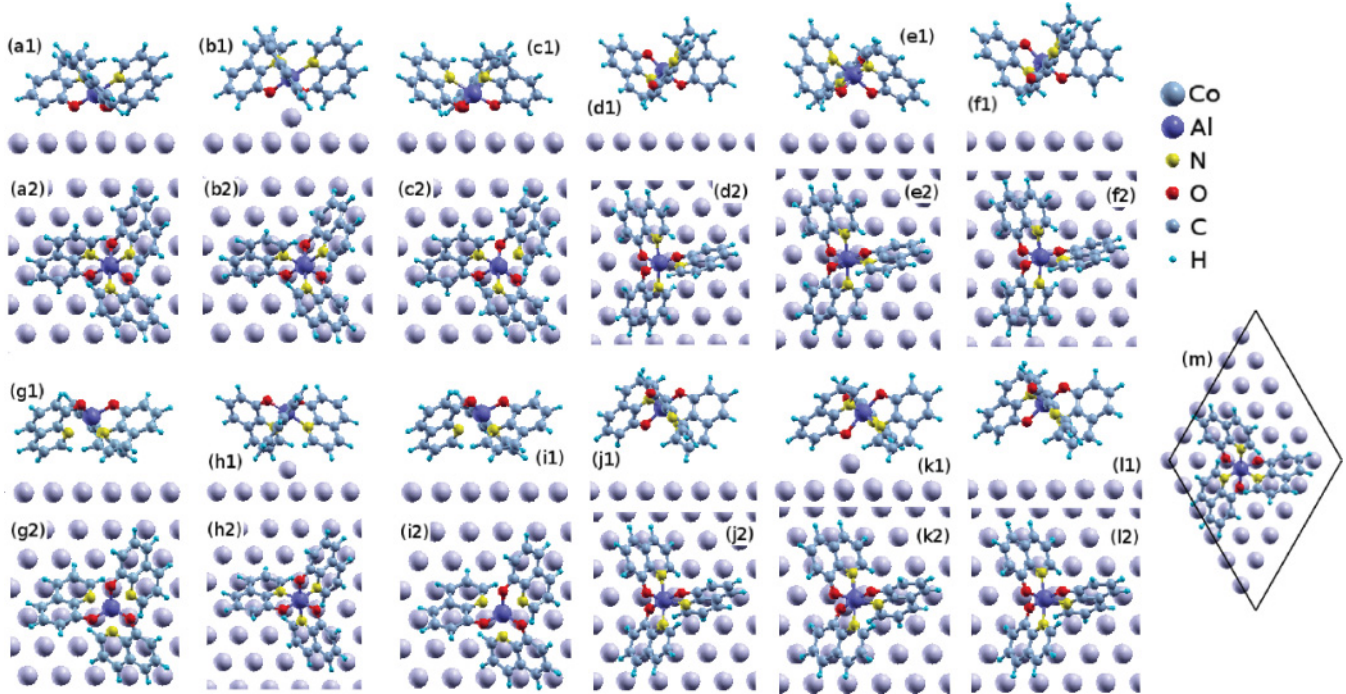


FIG. 2. (Color online) Side (1) and top (2) views of adsorption configurations: (a) fac-up/smooth, (b) fac-up/adatom, (c) fac-up/vacancy, (d) meri-up/smooth, (e) meri-up/adatom, (f) meri-up/vacancy, (g) fac-down/smooth, (h) fac-down/adatom, (i) fac-down/vacancy, (j) meri-down/smooth, (k) meri-down/adatom, and (l) meri-down/vacancy. The top view of the unit cell used in calculations is shown in (m), where the fac-up/smooth configuration is used as an example.

because the dispersion correction term in Eq. (1) is pairwise additive, the dispersion interaction between the Alq_3 molecule and the cobalt surface can be calculated by Eq. (1). For fac-up/adatom, meri-up/adatom, and meri-down/adatom configurations, DFT-D adsorption energies are larger by more than 0.5 eV than dispersion interaction energies between surface and molecule, which indicates chemical bonds are important in these configurations. The charge redistribution in real space of these configurations is illustrated in Fig. 3.

Adsorption energies (E_{ad}) and bonding energies (E_b) for all configurations calculated by the DFT-D method are listed in the left three columns of Table II. Adsorption energies as well as bonding energies for up configurations are larger than those of corresponding down configurations. This observation indicates the binding at the Alq_3/Co interface is dominated by the O-Co chemical bonds, which is consistent with experimental observations that Alq_3 molecules contact with a cobalt surface via oxygen atoms.¹⁴ In the up configurations, more O atoms can contact with the cobalt surface and form the O-Co chemical bonds than in the corresponding down configurations. The O-Co chemical bond formation at an Alq_3/Co interface is similar to the O-Mg bond at an Alq_3/Mg interface (Ref. 24) and the O-Al bond at an Alq_3/Al (Ref. 21) interface. Bonding energies of up/adatom configurations are larger than corresponding up/smooth and up/vacancy configurations, because chemical bonds between oxygen and cobalt adatoms are stronger than O-Co bonds formed at up/smooth and up/vacancy configurations. Except for down/adatom configurations, adsorption energies of facial Alq_3 on cobalt surfaces are lower than that of the meridional isomer, which indicates adsorption on the cobalt surface may alter the relative thermal stability between

facial and meridional Alq_3 isomers. However, one cannot arrive at the conclusion that a facial instead of a meridional isomer exists on the cobalt surface because of the relatively high energy barrier for facial-meridional isomerization in the gas phase.⁶⁶ The magnetic moments of atoms were calculated using Löwdin orthogonalization and population analysis.^{36,37} Magnetizations of Alq_3 molecules of meri-down/smooth and meri-down/vacancy configurations are negative (antiparallel to the magnetic moment of the cobalt surface), but in all other configurations the Alq_3 molecule has positive magnetization (parallel to the magnetic moment of the cobalt surface), ranging from $0.03\mu_B$ to $0.13\mu_B$.

IV. ANALYSIS AND DISCUSSION

A. Dispersion correction

Although computationally very efficient, the DFT-D scheme has an obvious weakness: the influence of orbital hybridization on the effective polarizability of atoms is neglected. In principle, the DFT-D scheme is fairly good for neutral organic systems, because atoms with the same atomic number tend to have very similar dispersion coefficients in these systems.⁶⁷ However, the DFT-D scheme could introduce problems for metal surfaces because the screening effect, which reduces the effective polarizability of metals that are far away from the surface, is not included.^{43,68}

In the following, we discuss the effect of the dispersion correction in “up” configurations, which are more stable than “down” configurations. The GGA exchange-correlation functional without dispersion correction was used to obtain fully relaxed structures for these configurations (labeled as

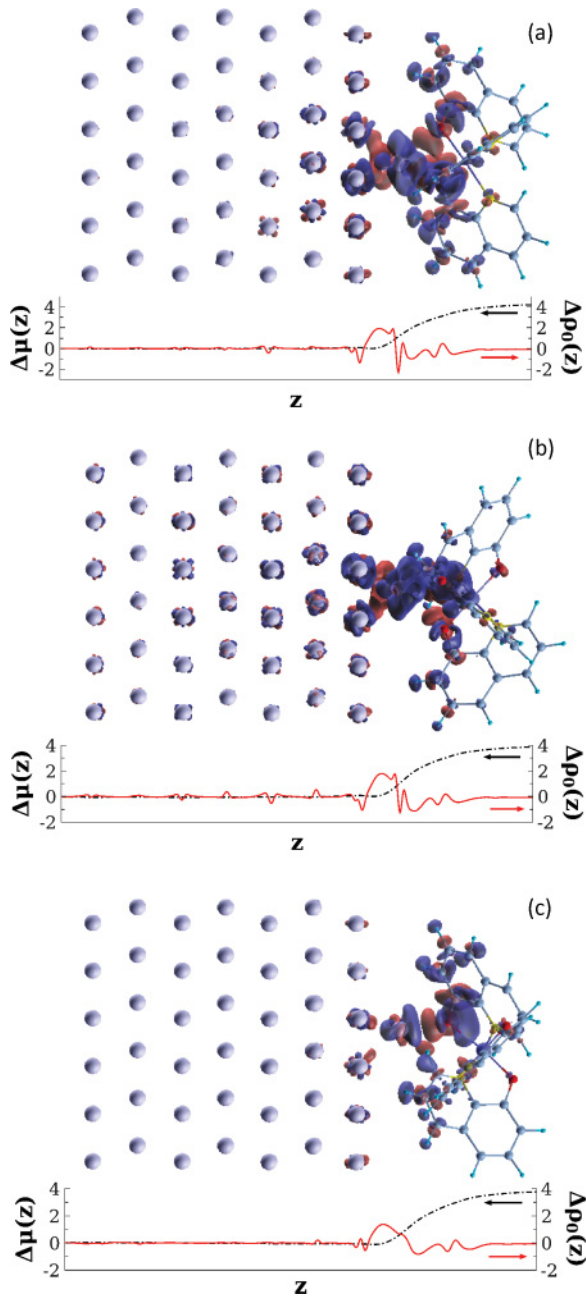


FIG. 3. (Color online) Charge transfer at Alq_3/Co interface (upper panel, isovalues: $+10 \text{ nm}^{-3}$ and -10 nm^{-3} for red and blue, respectively), averaged charge transfer over x - y plane (solid line, in nm^{-3}), and interface dipole (dot-dashed line, in debye), for (a) fac-up/adatom, (b) meri-up/adatom, and (c) meri-down/adatom configurations.

0L in Table III). Without the dispersion term, adsorption energies of fac-up configurations are smaller than those of meri-up, which is in contrast with DFT-D results. Because of dispersion interaction between Alq_3 molecule and cobalt surface, optimized position of Alq_3 molecules by DFT-D method are shifted toward cobalt surface by 0.14–0.20 Å for meri-up and fac-up configurations compared to optimized position calculated by GGA method.

To take into consideration the reduced dispersion coefficients due to screening, we calculated dispersion interaction

TABLE II. Calculation results of Alq_3 molecule adsorption on cobalt surfaces by DFT-D method. E_{ad} , adsorption energy; E_b , bonding energy; W , work function of the Alq_3 -molecule-decorated cobalt surfaces; μ , magnetization of the Alq_3 molecule; and Δq , charge transferred from the cobalt surface to the Alq_3 molecule.

Configuration	E_{ad} (eV)	E_b (eV)	W (eV)	μ (μ_B)	Δq (e^-)
Fac-up/smooth	2.43	2.88	2.93	0.07	0.83
Fac-down/smooth	1.67	1.94	5.39	0.11	0.48
Fac-up/adatom	2.47	3.71	2.72	0.03	0.60
Fac-down/adatom	1.52	2.54	5.39	0.09	0.29
Fac-up/vacancy	2.39	2.82	2.94	0.07	0.80
Fac-down/vacancy	1.59	1.79	5.43	0.11	0.39
Meri-up/smooth	1.01	1.06	4.42	0.05	0.12
Meri-down/smooth	0.97	0.97	4.86	-0.18	0.16
Meri-up/adatom	2.07	3.76	3.44	0.02	0.58
Meri-down/adatom	1.90	2.58	4.29	0.02	0.46
Meri-up/vacancy	1.00	1.01	4.42	0.13	0.08
Meri-down/vacancy	0.93	1.00	4.86	-0.16	0.13

energies between molecules and surface as a function of the number of cobalt layers in which DFT-D is applied. For a surface with an adatom or vacancy, the adatom or vacancy is included in the first layer. The corrected adsorption energies are listed in Table III. It can be seen that fac-up configurations become more stable than meri-up ones even if only the top layer of Co atoms is modeled by DFT-D. As the number of cobalt layers increases in the DFT-D scheme, the fac-up configurations gain more stability.

B. Dipole correction

The dipole correction³⁸ is essential to obtain correct adsorption energies of Alq_3 molecules on cobalt surfaces. In a first calculation, we performed geometry relaxations using the GGA method, and the difference between the adsorption geometries by calculation with and without the

TABLE III. Adsorption energies for fully relaxed configurations using GGA without dispersion correction (0L) and using the DFT-D method (7L); adsorption energies of Alq_3 molecules considering only dispersion interaction with the topmost layer (1L), with the topmost two layers (2L), and with the topmost three layers (3L) (in units of eV).

Configuration	0L	1L	2L	3L	7L
Fac-up/smooth	0.16	1.96	2.28	2.37	2.43
Meri-up/smooth	0.22	0.80	0.92	0.98	1.01
Fac-up/adatom	1.15	2.17	2.36	2.42	2.47
Meri-up/adatom	1.19	1.75	1.96	2.02	2.07
Fac-up/vacancy	0.21	1.89	2.25	2.32	2.39
Meri-up/vacancy	0.25	0.77	0.90	0.98	1.00
Fac-down/smooth	-0.21	1.27	1.54	1.61	1.67
Meri-down/smooth	0.20	0.75	0.88	0.94	0.97
Fac-down/adatom	0.18	1.24	1.41	1.50	1.52
Meri-down/adatom	0.55	1.61	1.79	1.87	1.90
Fac-down/vacancy	-0.05	1.21	1.46	1.54	1.59
Meri-down/vacancy	0.21	0.72	0.85	0.90	0.93

dipole correction is smaller than 0.01 Å. The adsorption energies obtained by GGA calculations without the dipole correction are about 0.2 eV higher than with the correction in the case of facial Alq₃ molecules on the different cobalt surfaces, but only by about 0.05 eV for the meridional isomer, because the dipole moment of the facial Alq₃ isomer is larger than that for the meridional Alq₃ isomer. We chose the direction perpendicular to the cobalt surface as the *z* axis. The angles between the *z* axis and the direction of electric dipole moments in the facial Alq₃ on the cobalt surfaces are nearly zero but are roughly 50° for the meridional isomer. The *z* components of the electric dipole moments of facial Alq₃ molecules are 7.2 D, which is larger than 2.6 (4.0 × cos 50°) D for the meridional isomer.

Work functions of Alq₃-molecule-covered cobalt surfaces also can only be obtained by calculations with the dipole correction. Facial Alq₃ molecules on a smooth cobalt surface are used as an example here. The work function of the surface is defined as the difference between the Fermi energy and the electrostatic energy away from the surface within the vacuum region. In the framework of pseudopotential theory, the electrostatic potential is the sum of the local effective potential and the electrostatic potential from valence electrons. The electrostatic potential from the pseudopotential calculation is identical to the all-electron electrostatic potential outside of core regions. To show the electrostatic potential in real space, the *x*-*y*-plane-averaged value was calculated and plotted along the *z* axis. The *x*-*y*-plane-averaged value of the electrostatic potential *V*_{es} is defined as

$$V_{es}(z) = \frac{1}{S} \iint V_{es}(x, y, z) dx dy, \quad (7)$$

where *S* is the area of the *x*-*y* cross section of the unit cell [Fig. 2(m)]. The calculated $-eV_{es}(z)$ with and without the dipole correction are shown in Fig. 4. In the vacuum region, the electrostatic energy without the dipole correction has a slope of 0.43 eV/nm. As a result, a vacuum energy level cannot be properly defined. The electric field was self-consistently calculated with the dipole correction to be 0.66 V/nm and the *x*-*y*-plane-averaged electrostatic energy shows a sharp jump at

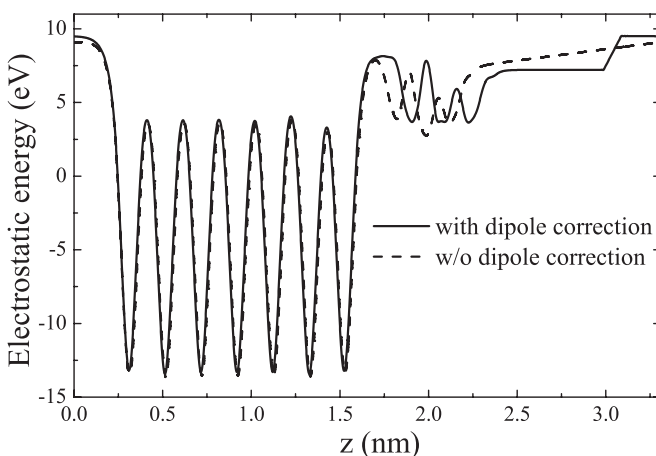


FIG. 4. The *x*-*y*-plane-averaged electrostatic energy of facial Alq₃ on a smooth cobalt surface, with dipole correction (solid line) and without dipole correction (dashed line).

the center of the vacuum region, as shown in Fig. 4. Except for this sharp jump, the *x*-*y*-plane-averaged electrostatic energy is ideally flat in the vacuum region, so different vacuum energy levels can be defined outside of the Alq₃-molecule-covered surface and outside of the smooth cobalt surface. The work functions for the two surfaces were calculated to be 2.94 and 5.02 eV, respectively, which were well reproduced by DFT-D calculations.

Taking into account depolarization of Alq₃ molecules by the electric field of neighboring adsorbates, the coverage dependence of the work-function shift is described by the Topping formula.⁶⁹ In fact, a simple linear function is a fairly good approximation.⁷⁰ We adopted the simple approximation here to estimate the work function for a cobalt surface covered by one monolayer of molecules; i.e., the coverage of an Alq₃ molecule on a cobalt surface is 100%. The coverage of Alq₃ molecules on cobalt surfaces is estimated to be 60% from the top view of a unit cell [Fig. 2(m)], and the work-function reduction was estimated to be 0.6 eV/60% = 1.0 eV in smooth/meri-up and vacancy/meri-up configurations. According to the experimentally observed work-function reduction after Alq₃ molecule deposition¹⁵ and the fact Alq₃ molecules favor *up* configurations,¹⁴ the most possible configuration of Alq₃ molecules on the cobalt surface was argued to be meri-up/smooth or meri-up/vacancy configurations.

C. Source of work-function changes

In the following, we discuss work functions of Alq₃-molecule-covered cobalt surfaces. There are two sources of work-function change by Alq₃ molecule adsorption: permanent electric dipoles of Alq₃ molecules (ΔW_{mol}), and charge redistribution at the interface (ΔW_{redist}). We use the fac-up/smooth configuration as an example to explain how ΔW_{mol} and ΔW_{redist} were calculated.

In this configuration, the electric dipole of the facial Alq₃ molecule points from the cobalt surface to vacuum, with the negative pole near the surface and the positive pole away from the surface. As a result, the work function of Alq₃-molecule-covered cobalt surfaces is reduced by the electric dipoles of the molecules. The electrostatic energy difference across the Alq₃ molecule layer $\Delta W_{mol} = -eV_{es}(+\infty) + eV_{es}(-\infty)$ is -1.28 eV, with $-eV_{es}(z)$ extracted from the facial Alq₃ molecule layer shown in the bottom panel in Fig. 5, where the geometry of the facial Alq₃ molecule was taken from the fully relaxed fac-up/smooth configuration.

The value of ΔW_{redist} results from charge redistribution at interface between the Alq₃ molecule and the cobalt surface. Charge redistribution near a molecule-covered surface is the combined result of the push-back effect^{71,72} and the polarization of the adsorbate.⁷² At the surfaces of metals, electrons extend out into vacuum and leave holes within the metals. Thus, an intrinsic electric dipole forms at a metal surface, which contributes positively to the work function. However, when molecules are adsorbed on the surface, charge at the interface coming from the metal will be pushed back by Pauli repulsion, and the push-back effect results in charge accumulation at the metal surface.^{71,72} The intrinsic dipole at the metal surface and hence the work function of the molecule-covered surface decreases. On the other hand, the

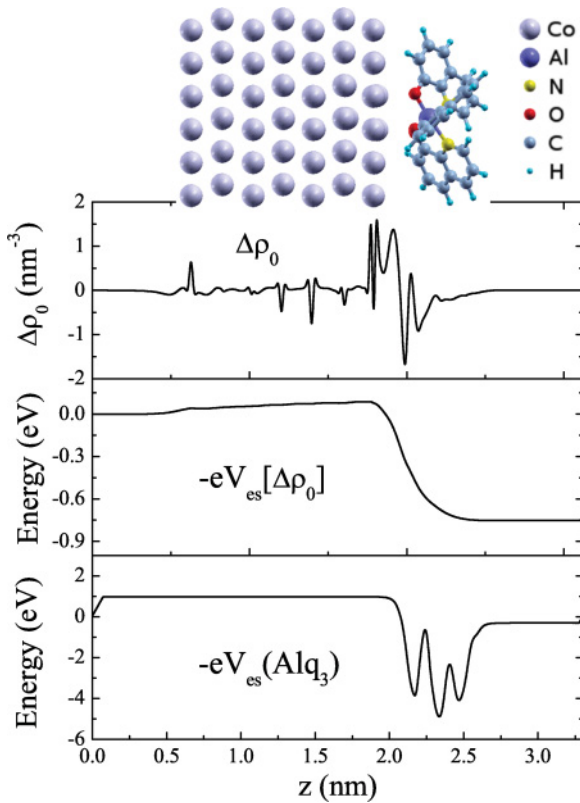


FIG. 5. (Color online) The x - y -plane-averaged charge redistribution (top) when facial Alq_3 molecules are adsorbed on a smooth cobalt surface (fac-up/smooth), the resulting electrostatic energy (middle), and the electrostatic energy of the facial Alq_3 molecule layer (bottom). Side view of fac-up/smooth configuration is illustrated by the topmost picture.

adsorbate feels the electrostatic field from the metal surface.⁷² The polarization of the adsorbate leads to charge transfer within the molecules and results in a charge accumulation on the metal side and charge depletion on the opposite side. The above qualitative analysis tells us there would be a charge accumulation near the cobalt surface and a charge depletion at the molecule side.

The charge redistribution due to molecule-surface interaction is defined as

$$\Delta\rho(\vec{r}) = \rho_{\text{mol+surf}}(\vec{r}) - \rho_{\text{mol}}(\vec{r}) - \rho_{\text{surf}}(\vec{r}), \quad (8)$$

where $\rho_{\text{mol+surf}}$ is the total charge density of the fully relaxed configuration and ρ_{mol} and ρ_{surf} are the charge densities of the bare molecule and surface.

In order to calculate ΔW_{redist} , the charge redistribution $\Delta\rho(\vec{r})$ [$\vec{r} = (x, y, z)$] is divided into two parts,

$$\Delta\rho(x, y, z) = \Delta\rho_0(z) + \Delta\rho_1(x, y, z), \quad (9)$$

where $\Delta\rho_0(z)$ is the x - y -plane-averaged value,

$$\Delta\rho_0(z) = \frac{1}{S} \iint \Delta\rho(x, y, z) dx dy \quad (10)$$

(S is the area of a unit cell in x - y plane), and

$$\Delta\rho_1(x, y, z) = \Delta\rho(x, y, z) - \Delta\rho_0(z), \quad (11)$$

TABLE IV. Work-function change by Alq_3 adsorption due to permanent electric dipole of Alq_3 molecules ΔW_{mol} and due to interface charge transfer ΔW_{redist} and their corresponding interface dipoles.

Configuration	ΔW_{mol} (eV)	μ_{mol} (D)	ΔW_{redist} (eV)	μ_{redist} (D)
Fac-up/smooth	-1.24	6.43	-0.76	3.94
Fac-down/smooth	1.01	-5.24	-0.53	2.75
Fac-up/adatom	-1.22	6.33	-0.82	4.25
Fac-down/adatom	1.09	-5.65	-0.46	2.39
Fac-up/vacancy	-1.26	6.53	-0.68	3.53
Fac-down/vacancy	1.06	-5.50	-0.50	2.59
Meri-up/smooth	-0.42	2.18	-0.08	0.41
Meri-down/smooth	0.41	-2.13	-0.47	2.44
Meri-up/adatom	-0.54	2.80	-0.75	3.89
Meri-down/adatom	0.30	-1.56	-0.73	3.78
Meri-up/vacancy	-0.42	2.18	-0.07	0.36
Meri-down/vacancy	0.40	-2.07	-0.43	2.23

with

$$\iint \Delta\rho_1(\vec{r}) dx dy = 0, \quad \forall z. \quad (12)$$

The electrostatic potential induced by $\Delta\rho_1$ decays exponentially into vacuum,³⁸ so hereafter this part is neglected. The interface dipole induced by charge redistribution is calculated as

$$\Delta\mu(z) = -S|e| \int \Delta\rho_0(z') (z' - z) dz'. \quad (13)$$

The interface dipole moments $\Delta\mu(z)$ for some configurations are plotted in Fig. 3, and interface dipoles due to charge redistribution calculated by $\mu_{\text{redist}} = \Delta\mu(+\infty) - \Delta\mu(-\infty)$ are listed in Table IV. The electrostatic potential induced by charge redistribution at the interface is calculated as

$$V_{\text{es}}[\Delta\rho_0](z) = -\frac{|e|}{2\epsilon_0} \int \Delta\rho_0(z') |z - z'| dz'. \quad (14)$$

The change in work function ΔW_{redist} was calculated as

$$\Delta W_{\text{redist}} = -eV_{\text{es}}(z = +\infty) + eV_{\text{es}}(z = -\infty). \quad (15)$$

The x - y -plane-averaged charge redistribution $\Delta\rho_0(z)$ in the fac-up/smooth configuration is shown in the top panel of Fig. 5. It can be seen that charge redistribution within the cobalt slab region is negligible; charges accumulate near the Alq_3 /cobalt interface and deplete within the molecule region. The electrostatic energy $-eV_{\text{es}}[\Delta\rho_0](z)$ calculated by Eq. (14) is shown in the middle panel of Fig. 5 and ΔW_{redist} was calculated by Eq. (15) to be -0.76 eV.

Work-function changes due to permanent electric dipoles of Alq_3 molecules (ΔW_{mol}) and those resulting from interface charge redistribution (ΔW_{redist}) and their corresponding dipoles (μ_{mol} and μ_{redist}) are listed in Table IV. There is a linear relation between the interfacial electric dipole and the resulting work-function change:

$$\Delta W_a = \frac{-|e|\mu_a}{\epsilon_0 S}, \quad a = \text{mol,redist} \quad (16)$$

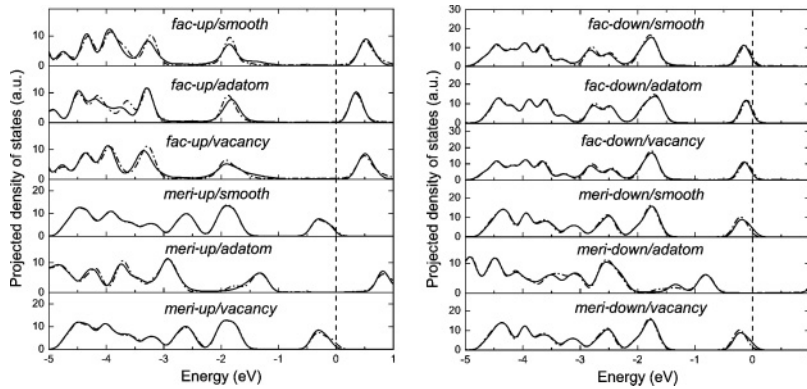


FIG. 6. Spin-polarized density of states projected onto the Alq_3 molecule (solid line, spin up; dash-dotted line, spin down). The Fermi energy level is set to zero.

(S is the area of unit-cell x - y cross section). Dipoles due to molecules are positive for up and negative for down configurations. Because Alq_3 molecules distort after adsorption and the directions of electric dipoles are not perpendicular to the cobalt surface, amplitudes of μ_{mol} are smaller than permanent electric dipoles of Alq_3 isomers. However, charge-redistribution-induced interface dipoles are always positive, consistent with the qualitative analysis above. Except for meri-up/smooth and meri-up/vacancy configurations, the amplitudes of charge-redistribution-induced interface dipoles are comparable to molecular dipoles in all configurations, which indicates that charge redistribution is non-negligible in determining the work function of Alq_3/Co surfaces. For meri-up/smooth and meri-up/vacancy configurations, the interface dipoles are dominated by molecular permanent dipoles, which is similar to Alq_3 adsorption on aluminum²¹ and magnesium²⁴ surfaces.

D. Energy-level alignment at surface

Molecular energy-level alignment at an Alq_3/Co interface is illustrated by the projected density of states (PDOS) onto the Alq_3 molecule, as shown in Fig. 6. The shapes of the PDOS in meri/adatom configurations are different from those in other configurations because of the strong interaction between Alq_3 molecules and the cobalt adatom. Except for meri/adatom configurations, the HOMO energy levels are located around 2 eV below the Fermi level, and the LUMO energy levels are around the Fermi level. The HOMO-LUMO gaps of isolated Alq_3 molecules are 1.9 eV for meridional and 2.1 eV for facial Alq_3 calculated by the GGA-PBE exchange-correlation functional. HOMO-LUMO gaps for Alq_3 molecules adsorbed on cobalt surfaces (Fig. 6) are around 2.0 eV for all configurations, which is close to those of isolated Alq_3 isomers. However, there is visible broadening, splitting, or shift for Alq_3 PDOS peaks in the Alq_3/Co system compared to that of isolated Alq_3 molecules. As a result, Alq_3 molecules chemisorb on the cobalt surface, which is consistent with a relatively large amount of charge transfer, although the van der Waals dispersion interaction is important for adsorption energy. In Ref. 15, the HOMO-LUMO gap of an Alq_3 molecule was estimated to be about 2.8 eV. Recently, the HOMO-LUMO gap was directly measured to be 4.8 eV.²⁸ Our calculated HOMO-LUMO gap is smaller than that observed experimentally, which can be attributed to the GGA exchange-correlation potential we employed in this

work.⁷³ Linear-response time-dependent density functional theory or many-body perturbation theory is necessary to reproduce experimental photoelectron spectroscopy. Although positions of unoccupied orbitals calculated by the GGA exchange-correlation functional cannot be compared directly with experimental photoelectron spectroscopy, the calculated position of the HOMO energy level is in good agreement with experiment; in fact, Zhan *et al.*¹⁵ observed the HOMO energy level to be 2.1 eV lower than the Fermi level of the cobalt surface. The position of the HOMO energy level was predicted to be dependent on the orientation of an Alq_3 molecule on aluminum²¹ and on magnesium²⁴ surfaces. However, our calculations on the Alq_3/Co system show HOMO energy levels depend only weakly on the orientation of the Alq_3 molecule except for the meri/adatom configurations.

V. SUMMARY

The adsorption of Alq_3 molecules on a cobalt surface was investigated by first-principles methods. The van der Waals interaction is included by the DFT dispersion correction method. We calculated the adsorption energy, work function, and charge transfer of the Alq_3/Co system as well as magnetizations of Alq_3 molecules on a cobalt surface in 12 possible configurations. We have considered two different isomers of the Alq_3 molecule (facial and meridional) and two different directions of the Alq_3 electric dipole (toward and away from the cobalt surface). In addition, three types of cobalt surfaces were considered: a smooth surface, a surface with an adatom, and a surface with a vacancy. Magnetizations of Alq_3 molecules are positive except in the meri-down/vacancy and meri-down/smooth configurations. The work function of the cobalt surface is modified by Alq_3 molecule adsorption due to permanent electric dipoles of molecules and charge redistribution at the Alq_3/Co interface. Electric dipoles resulting from charge redistribution are always positive in all configurations. According to experimental observations,¹⁵ the most likely configurations are meri-up/smooth and meri-up/vacancy configurations. The calculated position of the HOMO energy level of the Alq_3 molecule is consistent with experimental observations.¹⁵

ACKNOWLEDGMENTS

The project was supported by the State Key Project of Fundamental Research of the Ministry of Science and

Technology (MOST, Grant No. 2010CB934400) and the National Natural Science Foundation of China (NSFC, Grants No. 10934099 and No. 51021061), US DOE Grant No. BES

DE-FG02-02ER45995 (Y.-N.W., and H.-P.C.), and the partial support of the K. C. Wong Education Foundation, Hong Kong. The calculations were performed on NERSC computers.

¹M. N. Baibich, J. M. Broto, A. Fert, F. Nguyen Van Dau, F. Petroff, P. Etienne, G. Creuzet, A. Friederich, and J. Chazelas, *Phys. Rev. Lett.* **61**, 2472 (1988).

²J. S. Moodera, L. R. Kinder, T. M. Wong, and R. Meservey, *Phys. Rev. Lett.* **74**, 3273 (1995).

³V. Dedić, M. Murgia, F. C. Matacotta, C. Taliani, and S. Barbanera, *Solid State Commun.* **122**, 181 (2002).

⁴Z. H. Xiong, D. Wu, Z. V. Vardeny, and J. Shi, *Nature (London)* **427**, 821 (2004).

⁵C. Barraud, P. Seneor, R. Mattana, S. Fusil, K. Bouzehouane, C. Deranlot, P. Graziosi, L. Hueso, I. Bergenti, V. Dedić, F. Petroff, and A. Fert, *Nat. Phys.* **6**, 615 (2010).

⁶T. X. Wang, H. X. Wei, Z. M. Zeng, X. F. Han, Z. M. Hong, and G. Q. Shi, *Appl. Phys. Lett.* **88**, 242505 (2006).

⁷D. Liu, Y. Hu, H. Guo, and X. F. Han, *Phys. Rev. B* **78**, 193307 (2008).

⁸J. J. H. M. Schoonus, P. G. E. Lumens, W. Wagemans, J. T. Kohlhepp, P. A. Bobbert, H. J. M. Swagten, and B. Koopmans, *Phys. Rev. Lett.* **103**, 146601 (2009).

⁹V. Dedić, L. E. Hueso, I. Bergenti, A. Riminucci, F. Borgatti, P. Graziosi, C. Newby, F. Casoli, M. P. De Jong, C. Taliani, and Y. Zhan, *Phys. Rev. B* **78**, 115203 (2008).

¹⁰T. S. Santos, J. S. Lee, P. Middal, I. C. Lekshmi, B. Satpati, and J. S. Moodera, *Phys. Rev. Lett.* **98**, 016601 (2007).

¹¹Y. L. Chan, Y. J. Hung, C. H. Wang, Y. C. Lin, C. Y. Chiu, Y. L. Lai, H. T. Chang, C. H. Lee, Y. J. Hsu, and D. H. Wei, *Phys. Rev. Lett.* **104**, 177204 (2010).

¹²D. Sun, L. Yin, C. Sun, H. Guo, Z. Gai, X.-G. Zhang, T. Z. Ward, Z. Cheng, and J. Shen, *Phys. Rev. Lett.* **104**, 236602 (2010).

¹³F. Borgatti, I. Bergenti, F. Bona, V. Dedić, A. Fondacaro, S. Huotari, G. Monaco, D. A. MacLaren, J. N. Chapman, and G. Panaccione, *Appl. Phys. Lett.* **96**, 043306 (2010).

¹⁴A. N. Caruso, D. L. Schulz, and P. A. Dowben, *Chem. Phys. Lett.* **413**, 321 (2005).

¹⁵Y. Q. Zhan, M. P. de Jong, F. H. Li, V. Dedić, M. Fahlman, and W. R. Salaneck, *Phys. Rev. B* **78**, 045208 (2008).

¹⁶W. Xu, J. Brauer, G. Szulczewski, M. S. Driver, and A. N. Caruso, *Appl. Phys. Lett.* **94**, 233302 (2009).

¹⁷N. Atodiresei, J. Brede, P. Lazić, V. Caciuc, G. Hoffmann, R. Wiesendanger, and S. Blügel, *Phys. Rev. Lett.* **105**, 066601 (2010).

¹⁸R. H. Friend, R. W. Gymer, A. B. Holmes, J. H. Burroughes, R. N. Marks, C. Taliani, D. D. C. Bradley, D. A. D. Santos, J. L. Brédas, M. Lögglund, and W. R. Salaneck, *Nature (London)* **397**, 121 (1999).

¹⁹A. Curioni and W. Andreoni, *Synth. Met.* **111-112**, 299 (2000).

²⁰C. Shen, A. Kahn, and J. Schwartz, *J. Appl. Phys.* **89**, 449 (2001).

²¹S. Yanagisawa and Y. Morikawa, *Chem. Phys. Lett.* **420**, 523 (2006).

²²S. Yanagisawa and Y. Morikawa, *Jpn. J. Appl. Phys.* **45**, 413 (2006).

²³S. Yanagisawa, K. Lee, and Y. Morikawa, *J. Chem. Phys.* **128**, 244704 (2008).

²⁴S. Yanagisawa and Y. Morikawa, *J. Phys.: Condens. Matter* **21**, 064247 (2009).

²⁵S. Yanagisawa, I. Hamada, K. Lee, D. C. Langreth, and Y. Morikawa, *Phys. Rev. B* **83**, 235412 (2011).

²⁶H. Ishii, K. Sugiyama, E. Ito, and K. Seki, *Adv. Mater.* **11**, 605 (1999).

²⁷Y. Zhan, E. Holmström, R. Lizárraga, O. Eriksson, X. Liu, F. Li, E. Carlegrim, S. Stafström, and M. Fahlman, *Adv. Mater.* **22**, 1626 (2010).

²⁸J. S. Jiang, J. E. Pearson, and S. D. Bader, *Phys. Rev. Lett.* **106**, 156807 (2011).

²⁹S. Pramanik, C. G. Stefanita, S. Patibandla, S. Bandyopadhyay, K. Garre, N. Harth, and M. Cahay, *Nat. Nanotechnol.* **2**, 216 (2007).

³⁰M. Jergel, I. Cheshko, Y. Halahovets, P. Šiffalovič, I. Mat'ko, R. Senderák, S. Protsenko, E. Majková, and Š. Luby, *J. Phys. D: Appl. Phys.* **42**, 135406 (2009).

³¹P. Giannozzi, S. Baroni, N. Bonini, M. Calandra, R. Car, C. Cavazzoni, D. Ceresoli, G. L. Chiarotti, M. Cococcioni, I. Dabo, A. D. Corso, S. Fabris, G. Fratesi, S. de Gironcoli, R. Gebauer, U. Gerstmann, C. Gougaussis, A. Kokalj, M. Lazzeri, L. Martin-Samos, F. M. N. Marzari, R. Mazzarello, S. Paolini, A. Pasquarello, L. Paulatto, C. Sbraccia, S. Scandolo, G. Sclauzero, A. P. Seitsonen, P. U. A. Smogunov, and R. M. Wentzcovitch, *J. Phys.: Condens. Matter* **21**, 395502 (2009).

³²J. P. Perdew, K. Burke, and M. Ernzerhof, *Phys. Rev. Lett.* **77**, 3865 (1996).

³³D. Vanderbilt, *Phys. Rev. B* **41**, 7892 (1990).

³⁴<http://www.quantum-espresso.org>.

³⁵F. Ono and H. Maeta, *J. Phys. Colloques* **49**, C8 (1988).

³⁶P. P. Löwdin, *J. Chem. Phys.* **18**, 365 (1950).

³⁷P. P. Löwdin, *Adv. Phys.* **5**, 1 (1956).

³⁸L. Bengtsson, *Phys. Rev. B* **59**, 12301 (1999).

³⁹P. Sony, P. Puschnig, D. Nabok, and C. Ambrosch-Draxl, *Phys. Rev. Lett.* **99**, 176401 (2007).

⁴⁰N. Atodiresei, V. Caciuc, P. Lazić, and S. Blügel, *Phys. Rev. Lett.* **102**, 136809 (2009).

⁴¹M. Vanin, J. J. Mortensen, A. K. Kelkkanen, J. M. Garcia-Lastra, K. S. Thygesen, and K. W. Jacobsen, *Phys. Rev. B* **81**, 081408(R) (2010).

⁴²M. Mura, A. Gulans, T. Thonhauser, and L. Kantorovich, *PhysChemChemPhys* **12**, 4759 (2010).

⁴³E. R. McNellis, J. Meyer, and K. Reuter, *Phys. Rev. B* **80**, 205414 (2009).

⁴⁴V. R. Cooper, L. Kong, and D. C. Langreth, *Phys. Procedia* **3**, 1417 (2010).

⁴⁵Q. Wu and W. Yang, *J. Chem. Phys.* **116**, 515 (2002).

⁴⁶F. Ortmann, F. Bechstedt, and W. G. Schmidt, *Phys. Rev. B* **73**, 205101 (2006).

⁴⁷F. Ortmann, W. G. Schmidt, and F. Bechstedt, *Phys. Rev. Lett.* **95**, 186101 (2005).

⁴⁸S. Grimme, *J. Comput. Chem.* **27**, 1787 (2006).

⁴⁹A. Tkatchenko and M. Scheffler, *Phys. Rev. Lett.* **102**, 073005 (2009).

⁵⁰M. Dion, H. Rydberg, E. Schroder, D. C. Langreth, and B. I. Lundqvist, *Phys. Rev. Lett.* **92**, 246401 (2004).

⁵¹G. Román-Pérez and J. M. Soler, *Phys. Rev. Lett.* **103**, 096102 (2009).

⁵²K. Lee, É. D. Murray, L. Kong, B. I. Lundqvist, and D. C. Langreth, *Phys. Rev. B* **82**, 081101(R) (2010).

⁵³S. Grimme, *Wiley Interdiscip. Rev.: Comput. Mol. Sci.* **1**, 211 (2011).

⁵⁴A. Curioni, M. Boero, and W. Andreoni, *Chem. Phys. Lett.* **294**, 263 (1998).

⁵⁵M. Cölle, R. E. Dinnebier, and W. Brüttig, *Chem. Commun.* 2908 (2002).

⁵⁶M. Brinkmann, G. Gadret, M. Muccini, C. Taliani, N. Masciocchi, and A. Sironi, *J. Am. Chem. Soc.* **122**, 5147 (2000).

⁵⁷M. D. Halls and H. B. Schlegel, *Chem. Mater.* **13**, 2632 (2001).

⁵⁸K. Tarafder, B. Sanyal, and P. M. Oppeneer, *Phys. Rev. B* **82**, 060413 (2010).

⁵⁹R. L. Martin, J. D. Kress, I. H. Campbell, and D. L. Smith, *Phys. Rev. B* **61**, 15804 (2000).

⁶⁰H. Kaji, Y. Kusaka, G. Onoyama, and F. Horii, *J. Am. Chem. Soc.* **128**, 4292 (2006).

⁶¹R. Katakura and Y. Koide, *Inorg. Chem.* **45**, 5730 (2006).

⁶²A. Curioni and W. Andreoni, *J. Am. Chem. Soc.* **121**, 8216 (1999).

⁶³G. P. Kushto, Y. Iizumi, J. Kido, and Z. H. Kafafi, *J. Phys. Chem. A* **104**, 3670 (2000).

⁶⁴O. Hjortstam, J. Trygg, J. M. Wills, B. Johansson, and O. Eriksson, *Phys. Rev. B* **53**, 9204 (1996).

⁶⁵H. B. Michaelson, *J. Appl. Phys.* **48**, 4729 (1977).

⁶⁶M. Utz, C. Chen, M. Morton, and F. Papadimitrakopoulos, *J. Am. Chem. Soc.* **125**, 1371 (2003).

⁶⁷E. R. Johnson, I. D. Mackie, and G. A. DiLabio, *J. Phys. Org. Chem.* **22**, 1127 (2009).

⁶⁸G. Mercurio, E. R. McEllis, I. Martin, S. Hagen, F. Leyssner, S. Soubatch, J. Meyer, M. Wolf, P. Tegeder, F. S. Tautz, and K. Reuter, *Phys. Rev. Lett.* **104**, 036102 (2010).

⁶⁹J. Topping, *Proc. R. Soc. London A* **114**, 67 (1927).

⁷⁰V. De Renzi, R. Rousseau, D. Marchetto, R. Biagi, S. Scandolo, and U. del Pennino, *Phys. Rev. Lett.* **95**, 046804 (2005).

⁷¹N. D. Lang and W. Kohn, *Phys. Rev. B* **1**, 4555 (1970).

⁷²X. Crispin, V. Geskin, A. Crispin, J. Cornil, R. Lazzaroni, W. R. Salaneck, and J. Brédas, *J. Am. Chem. Soc.* **124**, 8131 (2002).

⁷³J. B. Neaton, M. S. Hybertsen, and S. G. Louie, *Phys. Rev. Lett.* **97**, 216405 (2006).